fuels

MDPI

Article

Activation of CO_2 on the Surfaces of Bare, Ti-Adsorbed and Ti-Doped C_{60}

Navaratnarajah Kuganathan

Department of Materials, Imperial College London, London SW7 2AZ, UK; n.kuganathan@imperial.ac.uk

Abstract: There is a growing interest in finding a suitable catalyst for the adsorption and activation of CO_2 molecules to minimize the effect of global warming. In this study, density functional theory-based simulations are employed to examine the adsorption and activation of a CO_2 molecule on the pure, Ti-supported and Ti-doped surfaces of C_{60}. The adsorption on the pure surface is very week. Adsorption becomes significant on the Ti-supported C_{60} surface together with significant activation. Such strong adsorption is evidenced by the significant charge transfer between Ti and C_{60}. The Ti-doped C_{60} surface adsorbs weakly, but the activation is not significant.

Keywords: activation; DFT; doping; C_{60}; adsorption; charge transfer

Citation: Kuganathan, N. Activation of CO_2 on the Surfaces of Bare, Ti-Adsorbed and Ti-Doped C_{60}. *Fuels* **2022**, *3*, 176–183. https://doi.org/10.3390/fuels3010011

Academic Editor: Javier Ereña Loizaga

Received: 1 February 2022
Accepted: 18 March 2022
Published: 19 March 2022

1. Introduction

Capture and adsorption of CO_2 is crucial towards global warming prevention and hydrogen production via purification of gas mixtures. A variety of materials including metal-organic frameworks [1–5], zeolites [6–9], metal oxides [10–12], organic polymers [13–15] and silica [16–18] have been used to investigate the efficacy of adsorbing CO_2.

Buckminsterfullerene (C_{60}) has gathered a lot of interest due to its wide range of properties such as high thermal, chemical and mechanical stability [19]. Both inner and outer surfaces of C_{60} have been thoroughly studied for encapsulation and adsorption of a variety of atoms and molecules respectively [20–25]. Alkali or transition metal adsorbed or doped C_{60} surfaces have been considered for the adsorption and the activation of small molecules such H_2, N_2 and CO_2 [20,22,23,25]. Transition metal-doped C_{60} structures have some special features over alkali atoms-doped C_{60}. They are size mismatch between highly charged metal ions and C_{60} and small lattice energies of hypothetical $M^{n+}-C_{60}{}^{n-}$ complexes. Titanium doped C_{60} has been studied experimentally and theoretically as a candidate catalyst to adsorb H_2 and activate N_2 molecules [22,23]. It is anticipated that Ti atom supported on a C_{60} molecule can introduce a charge transfer (Ti to C_{60}) due to the larger electronegativity of C_{60}. The positively charged Ti is expected to enhance the adsorption of CO_2 molecule via strong Ti−O bond formation.

Here, computational modelling based on the density functional theory (DFT) is used to examine the adsorption efficacy of a CO_2 molecule on the surfaces of pure, Ti-adsorbed and Ti-doped C_{60}. The current methodology enabled us to determine the relaxed configurations together with electronic structures and charges on the adsorbed or doped Ti or CO_2 molecule.

2. Computational Methods

A DFT simulation code VASP (Vienna ab initio simulation program) [26] was used to perform all calculations. Projected augmented wave (PAW) potentials [27] and plane wave basis sets (cut-off of 500 eV) were used. The exchange correlation term was modelled using the generalized gradient approximation (GGA) as parameterized by Perdew, Burke, and Ernzerhof (PBE) [28]. All structures were optimized using the conjugate gradient algorithm [29]. The forces on the atoms were less than 0.001 eV/Å. A supercell with a

dimension of 25 × 25 Å × 25 Å was used to ensure that the adjacent molecules do not interact with each other in all directions. A single Ti atom was considered at different positions on the surface of C_{60} for adsorption. The most favorable relaxed structure was allowed to interact a CO_2 molecule. Doping of Ti was carried out by replacing a C atom on the C_{60} molecule with Ti atom. A 2 × 2 × 2 Monk-horst k-point mesh [30] was used to relax all structures. Semi-empirical dispersive interactions were included as described by Grimme et al. [31] The charges on the atoms were calculated using the Bader charge analysis [32]. Adsorption energy was calculated for a CO_2 molecule interacting the C_{60} surface using the following equation.

$$E_{ads} = E_{CO_2} : C_{60} - E_{C_{60}} - E_{CO_2} \quad (1)$$

where $E_{CO_2} : C_{60}$ is the total energy of a CO_2 molecule interacting the surface of C_{60}, $E_{C_{60}}$ is the total energy of a C_{60} molecule and E_{CO_2} is the total energy of a CO_2 molecule.

3. Results

3.1. Strucure of C_{60}

C_{60} molecule is spherical and is formed by 12 pentagonal and 20 hexagonal molecules (see Figure 1a). It consists of two different carbon-carbon bonds (C–C and C=C) and their experimental values are reported to be 1.43 Å and 1.39 Å respectively [33]. First we optimized the *C_{60}* molecule to determine the equilibrium bond lengths to validate the pseudo potentials and basis sets used for C, Ti and O in this study. In the relaxed structure, the C–C and C=C bond distances were calculated to be 1.44 Å and 1.40 Å respectively, agreeing well with the corresponding experimental values. The calculated density of the states plot is shown in Figure 1b. The calculated gap between the highest occupied level and the lowest unoccupied level is 1.30 eV in a reasonable agreement with the values (1.55 eV and 1.63 eV) calculated in previous DFT simulations [34,35]. The underestimation of the band gap (E_{gap}) can be attributed to the failure of GGA functionals describing the exchange–correlation effect.

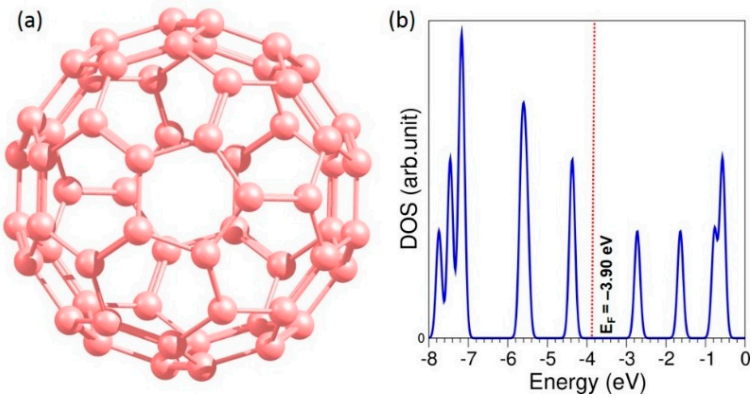

Figure 1. Relaxed structure of (**a**) C_{60} and (**b**) its DOS plot.

3.2. Encapsulation of CO_2 Inside the Pure C_{60}

A single CO_2 molecule was encapsulated and its encapsulation energy was calculated. Encapsulation is endoergic with and without dispersion (see Table 1). Dispersion improved the encapsulation by ~0.70 eV. A very small amount of charge is transferred between the CO_2 molecule and the C_{60} showing non-covalent interaction. The total DOS plot shows that the Fermi energy level and the value of the gap are almost unaffected (see Figure 2b). The charge density plot shows that there is no overlap between the CO_2 molecule and the inner wall of C_{60} (see Figure 2c).

Table 1. Encapsulation and Adsorption energy of a single CO_2 molecule.

System	Encapsulation Energy (eV)		Charge Transfer (e)	
	vdw-*free*	vdw	vdw-*free*	vdw
CO_2@C_{60}	1.60	0.94	–0.04	–0.04
	Adsorption energy (eV)		**Charge transfer (e)**	
CO_2_C_{60}	0.05	–0.05	–0.01	–0.02

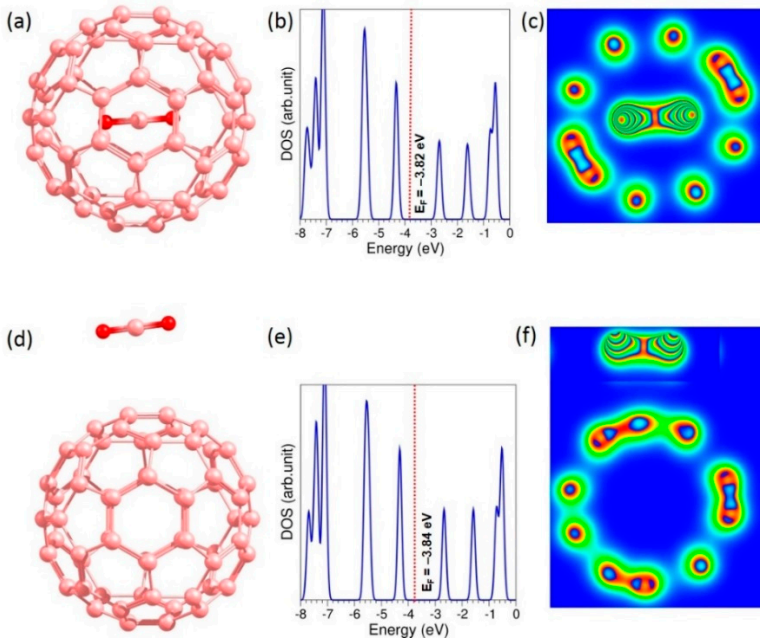

Figure 2. Relaxed structure of (**a**) a CO_2 molecule encapsulated inside the C_{60}, (**b**) its DOS plot and (**c**) charge density plot showing no interaction between the molecule and the inner wall of the C_{60}. Corresponding information (**d**–**f**) is also provided for a CO_2 molecule adsorbed on the surface of C_{60}.

3.3. Adsorption of CO_2 on the Surface of Pure C_{60}

The adsorption of CO_2 molecule was next considered. The relaxed structure is shown in Figure 2d. The adsorption is exoergic with dispersion and endoergic without dispersion, indicating the importance of dispersion (see Table 1). Charge transfer is negligible. The electronic structure is almost unaffected by the adsorption (see Figure 2e) as evidenced by the charge density plot in which there is no interaction of charge density (see Figure 2f).

3.4. Adsorption of CO_2 on the Surface of C_{60} Supported with Ti

Next, I considered a CO_2 molecule adsorbed on the Ti-supported C_{60} surface. Five different starting configurations were considered (see Figure 3) for the Ti interacting with C_{60}. In the configurations **H** and **P**, the Ti atom is positioned on the hexagonal ring and the pentagonal ring respectively. The configurations **66** and **65** accommodate the Ti atom above the bonds bridging hexagonal–hexagonal and hexagonal–pentagonal rings respectively. In the initial structure **C**, Ti atom is located above the C atom on the C_{60} surface. All initial configurations were fully relaxed. Table 2 lists the relative energies of the final configurations. The most stable configuration is found to be the configuration **H**. The inclusion of dispersion does not affect the trend in the relative energies.

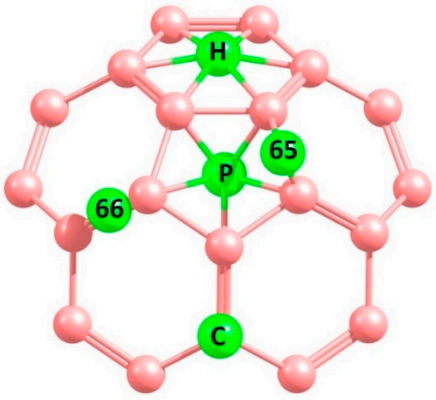

Figure 3. Five different initial sites (**H**, **P**, **66**, **65** and **C**) considered for the adsorption of a single Ti atom on the surface of C_{60}.

Table 2. Relative energies of five different configurations considered for the adsorption of Ti atom.

Structure	Relative Energy (eV)	
	vdw-*free*	vdw
H	**0.00**	**0.00**
C	0.42	0.42
66	0.42	0.42
P	0.58	0.59
65	0.84	0.82

The relaxed structure of Ti adsobed on the hexagonal ring of C_{60} (**H**) is shown in Figure 4a. The adsorbed Ti forms strond bonds with C in the hexagonal ring are described by the shorter Ti–C bond lenghts (see Figure 4b). The Bader charge analysis shows that there is a significant charge transfer from Ti to the C in the hexagonal ring (see Figure 4b). This is further confirmed by the positive Bader charge on the Ti atom and the negative Bader charges on the C. The adsorption energy was calculated using a Ti atom as a reference state. Adsorption is negative and its value is −1.71 eV with dispersion. Exclusion of dispersion reduces the adsorption by 0.04 eV as expected.

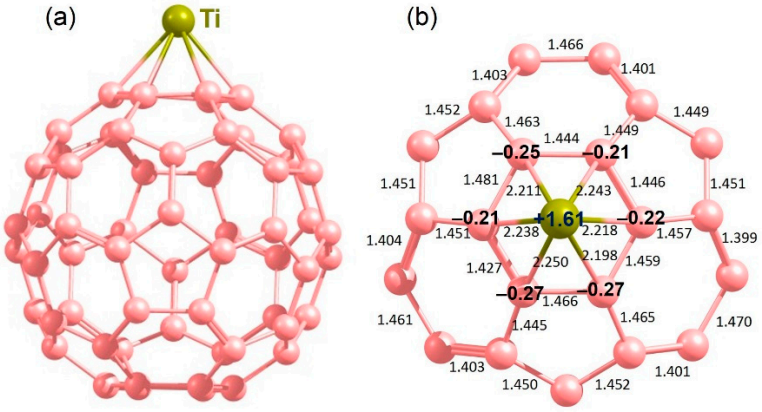

Figure 4. Optimized structure of (**a**) Ti atom adsorbed on the hexagonal ring of C_{60}, (**b**) bond lengths (Ti-C and C-C) and Bader charges on the Ti atom and the adjacent C atoms directly bonded to it.

The total DOS plot exhibits that the Ti-supported C_{60} is metallic (see Figure 5a). This is due to strong perturbation of C_{60} with Ti. The atomic DOS plots shows that the Fermi energy level is mainly populated with *d* states of Ti (see Figure 5b).

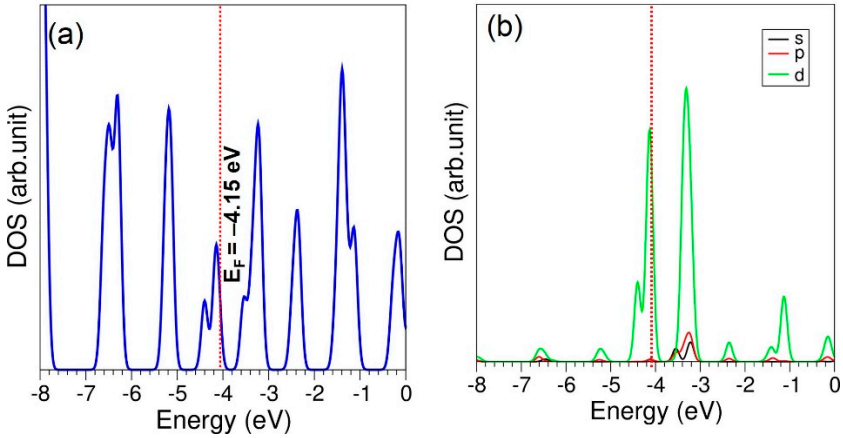

Figure 5. (**a**) Total DOS plot and (**b**) atomic DOS plot of Ti.

A single CO_2 molecule was allowed to adsorb on the surface of Ti-supported C_{60}. The relaxed configuration is shown in Figure 6a. In this structure, the CO_2 molecule exhibits a nonlinear structure. There is a significant elongation in the bond lengths of C-O in comparison with those found in molecular CO_2 (1.18 Å) (see Figure 6b). This indicates that depletion of CO_2 can be enhanced by the support of Ti on the surface of C_{60}. The Bader charge analysis shows that the net charge on the CO_2 molecule is −1.19.

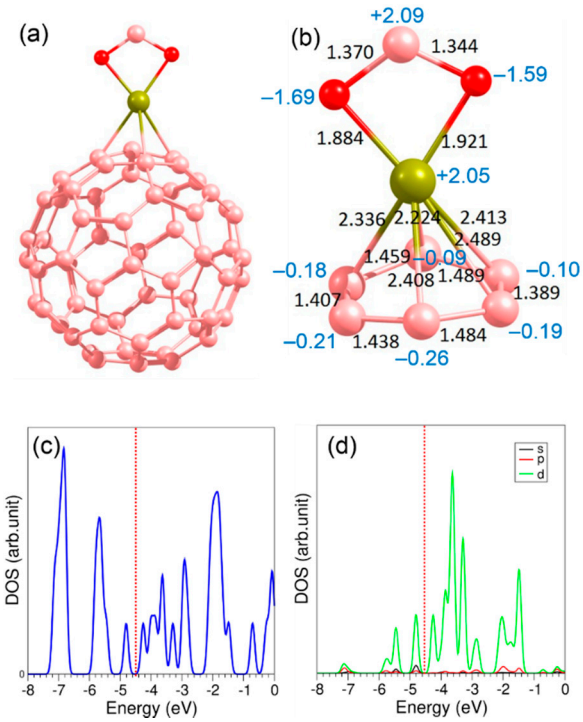

Figure 6. Relaxed structure of (**a**) a CO_2 molecule adsorbed on the Ti-supported surface, (**b**) bond distances and Bader charges on the atoms, (**c**) total DOS plot and (**d**) atomic DOS plot of Ti.

Adsorption energy of the CO_2 molecule was calculated. Adsorption is exoergic with an adsorption energy of −1.57 eV. Adsorption becomes less negative (by 0.06 eV) without dispersion. Adsorption is exoergic as confirmed by the strong bonding between Ti and oxygen in the CO_2 molecule. The resultant configuration exhibits a narrow-gap semiconductor (see Figure 6c). The states appearing around the Fermi level are contributed to by the *d* states of Ti (see Figure 6d).

3.5. Adsorption of CO_2 on the Surface Ti-Doped C_{60}

The efficacy of Ti-doped surface for the adsorption of CO_2 was next considered. The relaxed structure of Ti-doped C_{60} is shown in Figure 7a. In the relaxed structure, the Ti atom is displaced forming longer Ti−C bond lengths compared to C−C bond lengths (see Figure 7b). There is a significant distortion in the relaxed structure. The Bader charge analysis exhibits a significant charge transfer between Ti and three C atoms directly bonded to it. The Bader charge on the Ti is +2.21. The loss of 2.21 electrons is gained by three nearest neighbor C atoms. The total DOS plot exhibits that the resultant structure is a semi-conductor with a band gap of 0.6 eV. This value is lower than that found for the pure C_{60}. The atomic DOS plots shows that states near the Fermi level are mainly associated with the *d* sates of Ti.

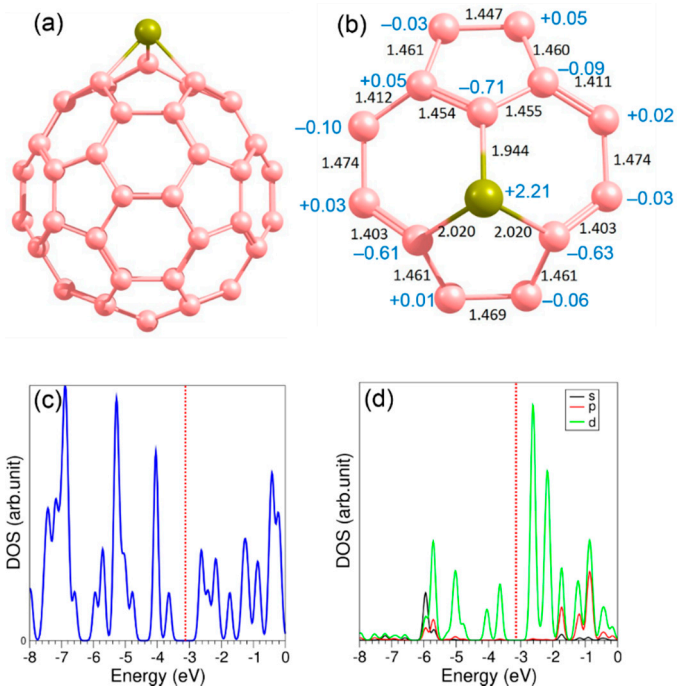

Figure 7. Relaxed structure of (**a**) Ti atom doped-C_{60}, (**b**) bond lengths (Ti-C and C-C) and Bader charges on the Ti atom and the adjacent C atoms directly bonded to it, (**c**) total DOS plot and (**d**) atomic DOS plot of Ti.

Adsorption of CO_2 was next considered on the surface of Ti-doped C_{60}. The relaxed structure is shown in Figure 8a. In the relaxed structure, one of the oxygen atoms in the CO_2 molecule forms a strong bond with Ti (see Figure 8b). In the relaxed structure, the CO_2 molecule is slightly bent. The net charge on the CO_2 molecule is −0.23 according to the Bader charge analysis. The activation of the C-O bond is not significant as its bond lengths are not significantly elongated with respect to its isolated molecule. The energy required to adsorb a CO_2 molecule is −0.41 eV with dispersion, indicating that Ti-doped C_{60} can accommodate a CO_2 molecule. Adsorption is endothermic without dispersion and its adsorption energy is +1.71 eV, again indicating the importance of dispersion. There is a small band gap of 0.50 eV observed in the total DOS plot. The states associated with the *d* orbitals of Ti are mainly localized near the Fermi energy level.

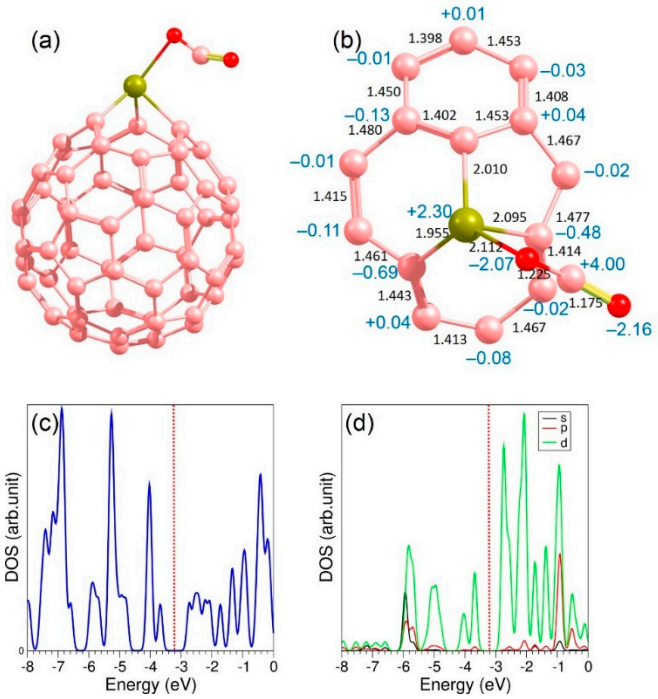

Figure 8. Relaxed structure showing (**a**) a CO_2 molecule adsorbed on the Ti-doped surface, (**b**) bond distances and Bader charges on the atoms, (**c**) total DOS plot and the (**d**) atomic DOS plot of Ti.

4. Conclusions

Computer simulations based on the DFT together with dispersion were applied to examine the efficacy of the pure, Ti-supported and Ti-doped C_{60} surface for the adsorption of a CO_2 molecule. The results show that there is no significant adsorption on the surface of pure C_{60}. Adsorption becomes significantly stronger once the Ti is supported on the surface of C_{60}. Such adsorption distorts and activates the CO_2 molecule significantly. The enhancement of adsorption is confirmed by the significant charge transfer between the Ti and the C_{60} molecule. Thus, the Ti-supported C_{60} molecule is the most efficient for CO_2 adsorption. The Ti-doped C_{60} surface has the ability to adsorb the CO_2 molecule. However, the activation is not significant.

Funding: This research received no external funding.

Data Availability Statement: The data presented in this study are available upon reasonable request from the author.

Acknowledgments: High performance computing center at Imperial College London is acknowledged for providing computational facilities.

Conflicts of Interest: The authors declare no conflict of interest.

References

1. Li, Z.; Liu, P.; Ou, C.; Dong, X. Porous Metal–Organic Frameworks for Carbon Dioxide Adsorption and Separation at Low Pressure. *ACS Sustain. Chem. Eng.* **2020**, *8*, 15378–15404. [CrossRef]
2. Trickett, C.A.; Helal, A.; Al-Maythalony, B.A.; Yamani, Z.H.; Cordova, K.E.; Yaghi, O.M. The chemistry of metal–organic frameworks for CO_2 capture, regeneration and conversion. *Nat. Rev. Mater.* **2017**, *2*, 17045. [CrossRef]
3. Gandara-Loe, J.; Pastor-Perez, L.; Bobadilla, L.F.; Odriozola, J.A.; Reina, T.R. Understanding the opportunities of metal–organic frameworks (MOFs) for CO_2 capture and gas-phase CO_2 conversion processes: A comprehensive overview. *React. Chem. Eng.* **2021**, *6*, 787–814. [CrossRef]
4. Liu, J.; Chen, C.; Zhang, K.; Zhang, L. Applications of metal–organic framework composites in CO_2 capture and conversion. *Chin. Chem. Lett.* **2021**, *32*, 649–659. [CrossRef]
5. Mahdipoor, H.R.; Halladj, R.; Ganji Babakhani, E.; Amjad-Iranagh, S.; Sadeghzadeh Ahari, J. Synthesis, characterization, and CO_2 adsorption properties of metal organic framework Fe-BDC. *RSC Adv.* **2021**, *11*, 5192–5203. [CrossRef]

6. Megías-Sayago, C.; Bingre, R.; Huang, L.; Lutzweiler, G.; Wang, Q.; Louis, B. CO_2 Adsorption Capacities in Zeolites and Layered Double Hydroxide Materials. *Front. Chem.* **2019**, *7*, 551. [CrossRef]
7. Bakhtyari, A.; Mofarahi, M.; Lee, C.-H. Chapter 9—CO_2 Adsorption by Conventional and Nanosized Zeolites. In *Advances in Carbon Capture*; Rahimpour, M.R., Farsi, M., Makarem, M.A., Eds.; Woodhead Publishing: Sawston, UK, 2020; pp. 193–228.
8. Hauchhum, L.; Mahanta, P. Carbon dioxide adsorption on zeolites and activated carbon by pressure swing adsorption in a fixed bed. *Int. J. Energy Environ. Eng.* **2014**, *5*, 349–356. [CrossRef]
9. Deng, Y.; Seville, J.P.K.; Bell, S.D.; Ingram, A.; Zhang, H.; Sweygers, N.; Dewil, R.; Baeyens, J.; Appels, L. Reviewing Fundamental CO_2 Adsorption Characteristics of Zeolite and Activated Carbon by In-situ Measurements With Radioactively Labelled CO_2. *Sep. Purif. Rev.* **2021**, *1*, 12.
10. Mutch, G.A.; Shulda, S.; McCue, A.J.; Menart, M.J.; Ciobanu, C.V.; Ngo, C.; Anderson, A.A.; Richards, M.R.; Vega-Maza, D. Carbon Capture by Metal Oxides: Unleashing the Potential of the (111) Facet. *J. Am. Chem. Soc.* **2018**, *140*, 4736–4742. [CrossRef]
11. Othman, F.E.C.; Yusof, N.; Samitsu, S.; Abdullah, N.; Hamid, M.F.; Nagai, K.; Nizam Zainal Abidin, M.; Ariff Azali, M.; Fauzi Ismail, A.; Jaafar, J.; et al. Activated carbon nanofibers incorporated metal oxides for CO_2 adsorption: Effects of different type of metal oxides. *J. CO2 Util.* **2021**, *45*, 101434. [CrossRef]
12. Irani, V.; Khosh, A.G.; Tavasoli, A. Polyethyleneimine (PEI) Functionalized Metal Oxide Nanoparticles Recovered From the Catalytic Converters of Spent Automotive Exhaust Systems and Application for CO_2 Adsorption. *Front. Energy Res.* **2020**, *8*, 196. [CrossRef]
13. Xu, C.; Yu, G.; Yuan, J.; Strømme, M.; Hedin, N. Microporous organic polymers as CO_2 adsorbents: Advances and challenges. *Mater. Today Adv.* **2020**, *6*, 100052. [CrossRef]
14. Jiangfei, G.; Lizhi, W.; Zhang, D.; Huang, J. Amino-Functionalized Porphyrin-Based Porous Organic Polymers for CO_2 Capture and Hg2+ Removal. *Energy Fuels* **2020**, *34*, 9771–9778. [CrossRef]
15. Patel, H.A.; Hyun Je, S.; Park, J.; Chen, D.P.; Jung, Y.; Yavuz, C.T.; Coskun, A. Unprecedented high-temperature CO_2 selectivity in N2-phobic nanoporous covalent organic polymers. *Nat. Commun.* **2013**, *4*, 1357. [CrossRef] [PubMed]
16. Zhao, G.; Aziz, B.; Hedin, N. Carbon dioxide adsorption on mesoporous silica surfaces containing amine-like motifs. *Appl. Energy* **2010**, *87*, 2907–2913. [CrossRef]
17. Kishor, R.; Ghoshal, A.K. Amine-Modified Mesoporous Silica for CO_2 Adsorption: The Role of Structural Parameters. *Ind. Eng. Chem. Res.* **2017**, *56*, 6078–6087. [CrossRef]
18. Yu, J.; Le, Y.; Cheng, B. Fabrication and CO_2 adsorption performance of bimodal porous silica hollow spheres with amine-modified surfaces. *RSC Adv.* **2012**, *2*, 6784–6791. [CrossRef]
19. Dresselhaus, M.S.; Dresselhaus, G.; Eklund, P.C. *Science of Fullerenes and Carbon Nanotubes*; Academic Press: San Diego, CA, USA, 1996.
20. Wang, Y.; Tománek, D.; Ruoff, R.S. Stability of M@C60 endohedral complexes. *Chem. Phys. Lett.* **1993**, *20*, 79–85. [CrossRef]
21. Brocławik, E.; Eilmes, A. Density functional study of endohedral complexes M@C60 (M=Li, Na, K, Be, Mg, Ca, La, B, Al): Electronic properties, ionization potentials, and electron affinities. *J. Chem. Phys.* **1998**, *108*, 3498–3503. [CrossRef]
22. Kuganathan, N.; Green, J.C.; Himmel, H.-J. Dinitrogen fixation and activation by Ti and Zr atoms, clusters and complexes. *New J. Chem.* **2006**, *30*, 1253–1262. [CrossRef]
23. Sun, Q.; Wang, Q.; Jena, P.; Kawazoe, Y. Clustering of Ti on a C60 Surface and Its Effect on Hydrogen Storage. *J. Am. Chem. Soc.* **2005**, *127*, 14582–14583. [CrossRef] [PubMed]
24. Mahdy, A.M.E. DFT study of hydrogen storage in Pd-decorated C60 fullerene. *Mol. Phys.* **2015**, *113*, 3531–3544. [CrossRef]
25. Gao, B.; Zhao, J.-X.; Cai, Q.-H.; Wang, X.-G.; Wang, X.-Z. Doping of Calcium in C60 Fullerene for Enhancing CO_2 Capture and N2O Transformation: A Theoretical Study. *J. Phys. Chem. A* **2011**, *115*, 9969–9976. [CrossRef] [PubMed]
26. Kresse, G.; Furthmüller, J. Efficient iterative schemes for ab initio total-energy calculations using a plane-wave basis set. *Phys. Rev. B* **1996**, *54*, 11169–11186. [CrossRef] [PubMed]
27. Blöchl, P.E. Projector augmented-wave method. *Phys. Rev. B* **1994**, *50*, 17953–17979. [CrossRef]
28. Perdew, J.P.; Burke, K.; Ernzerhof, M. Generalized Gradient Approximation Made Simple. *Phys. Rev. Lett.* **1996**, *77*, 3865–3868. [CrossRef] [PubMed]
29. Press, W.H.; Teukolsky, S.A.; Vetterling, W.T.; Flannery, B.P. Numerical Recipes. In *C: The Art of Scientific Computing*, 2nd ed.; Cambridge University Press: Cambridge, UK, 1992.
30. Monkhorst, H.J.; Pack, J.D. Special points for Brillouin-zone integrations. *Phys. Rev. B* **1976**, *13*, 5188–5192. [CrossRef]
31. Grimme, S.; Antony, J.; Ehrlich, S.; Krieg, H. A consistent and accurate ab initio parametrization of density functional dispersion correction (DFT-D) for the 94 elements H-Pu. *J. Chem. Phys.* **2010**, *132*, 154104. [CrossRef]
32. Bader, R.F.W. The zero-flux surface and the topological and quantum definitions of an atom in a molecule. *Theor. Chem. Acc.* **2001**, *105*, 276–283. [CrossRef]
33. Hawkins, J.M. Osmylation of C60: Proof and characterization of the soccer-ball framework. *Acc. Chem. Res.* **1992**, *25*, 150–156. [CrossRef]
34. Goclon, J.; Winkler, K.; Margraf, J.T. Theoretical investigation of interactions between palladium and fullerene in polymer. *RSC Adv.* **2017**, *7*, 2202–2210. [CrossRef]
35. Kuganathan, N.; Arya, A.K.; Rushton, M.J.D.; Grimes, R.W. Trapping of volatile fission products by C60. *Carbon* **2018**, *132*, 477–485. [CrossRef]